DEGREE PROGRAMME IN WIRELESS COMMUNICATIONS ENGINEERING

MASTER'S THESIS

Effect of Shadowing and Diffraction on the Received GNSS signal

Author	Md Rafiqul Islam
Supervisor	Adj. Prof. Markus Berg
Second Examiner	Dr. Marko Sonkki

May 2019

Islam Rafiqul. (2018) Effect of shadowing and diffraction on the received GNSS signal. University of Oulu, Degree Programme in Wireless Communications Engineering. Master's Thesis, 43p.

ABSTRACT

The characteristics of the GNSS received signal depend on the propagation medium environment. Typically, the transmitted signal interacts with several numbers of obstacles which leads to the multipath propagation to receiver end. In such cases, diffraction over the edges or wedges of the obstacles in the propagation path should be considered. The effects of diffraction and shadowing are the important elements in radio wave propagation because of their strong influence on the received signal quality. Especially, received signal strength and characteristics are very significant for GNSS applications.

This master's thesis investigates the effect of knife-edge diffraction model and shadowing environment on the received GNSS signal. Characterization of the received signal is investigated both theoretically and experimentally. In the measurement, a dual circular polarized antenna has been used to receive the multipath GPS signal in the shadow region in which antenna was placed in the zenith direction.

The measurement was performed for two scenarios 1) the receiver was in the static position, and 2) in motion for the second measurement. Measurement results show that, the received signals following the Knife-edge diffraction pattern for both measurements case.

In the first measurement case, knife-edge diffraction has been identified in received signal attenuation whereas the interference pattern in the LoS propagation can be observed because of multipath effect. In the deep shadow region, a linearly polarized signal has been received in both antennas because the incident RHCP signal turned into a linearly polarized signal after diffraction. For the second measurement case, knife-edge attenuation pattern is also visible.

A clear agreement between the measured and theoretical aspects has been achieved in the case of knife-edge diffraction.

Key words: GNSS, Diffraction, Shadowing, Path Loss, Knife-Edge Diffraction.

TABLE OF CONTENTS

FOREWORD

First of all, I would like to thank Allah for giving me the capability to finish this thesis work.

This work has been done as a part of the master's degree for Wireless Communication Engineering, University of Oulu, Finland.

I have learned many practical things as well as theoretical knowledge during this thesis work. I would like to express my gratitude to my supervisor Dr. Markus Berg for giving me an opportunity to work under his supervision. His continual supports during this thesis work and his instant responses to any queries have ended this thesis work on time. I would also like to thank my second examiner Dr. Marko Sonkki for his valuable comments that enhanced my thesis contents. Special thanks to Zeeshan Siddiqui and Mazidul Islam for their valuable suggestions.

I would like to thank my parent and my beloved Sultana for their love, supports and for always standing by me. This thesis would not have been possible without the love of my family.

I dedicate my thesis to my parents, wife and my little angel Nusaibah Binte Rafiq.

Oulu, June, 12 2019
Md Rafiqul Islam

LIST OF ABBREVIATIONS AND SYMBOLS

AR	Axial Ratio
BDS	BeiDou Navigation Satellite System
BPSK	Binary Phase Shift Keying
C/A	Coarse Acquisition
C/N0	Carrier to Noise Density
dB	Decibel
EMF	Electromotive Force
GNSS	Global Navigation Satellite System
GO	Geometrical Optics
IOC	Initial Operational Capability
LHCP	Left Hand Circular Polarized
LoS	Line of Sight
MEO	Medium Earth Orbit
NLoS	Non Line of Sight
PR	Pseudo Range
RHCP	Right Hand Circular Polarized
RTK	Real Time Kinematic
SNR	Signal-to-Noise Ratio
UAV	Unmanned Aerial Vehicle
UDT	Uniform Theory of Diffraction
XPI	Cross-Polarization Isolation
XPD	Cross-Polarization Discrimination

$g(\theta, \varphi)$	Element Factors
Z_a	Antenna Impedance
X_a	Antenna Reactance
R_a	Antenna Resistance
R_0	Skin Effect Resistance
R_r	Radiation Resistance
P_{rad}	Radiation Power
P_{in}	Input Power
$F(\theta, \varphi)$	Radiation Pattern

α	Receiver's Azimuth Angle
β	Diffraction Angle
ϕ	Azimuth Angle
η_{rad}	Radiation Efficiency
θ	Elevation Angle
φ	Phase Difference
θ_d	Diffraction Angle

Γ	Reflection Coefficient

1. INTRODUCTION

Global Navigation Satellite System (GNSS) is a wireless navigation system around the world. It is a key technology in the wireless navigation field which is improving the quality and safety of our daily life such as getting geolocation, safety operations in critical environments, speed up rescue operations, and so on. Due to the massive number of applications for navigation and positioning services, this system has been developed by reducing the multipath effects to signal interference [1], [2], [3].

GNSS satellites transmit electromagnetic waves consisted of two carriers (e.g. GPS transmits signal on two carrier frequencies 1575.42 MHz and 1227.60 MHz), two codes and a navigation message [4]. These are transmitted by the satellite antenna and received by user interface such as cellular tracking devices, car navigation systems, and aircraft tracking system. User's receiver obtains an estimate for the propagation time of the signal from the satellites to the receiver using modulated code (pseudo range) and phase of the signal carrier waves [5].

At least four satellites are required to get the receiver's location anywhere in the world. In the beginning, this technology was used to serve the only military purpose. Public service was allowed later in 1993. Nowadays, its popularity is increasing exponentially due to the various applications in different sectors such as ground mapping, transportation, Geospatial Information Systems (GIS), machine control, port automation, precision agriculture, timing, construction, marine, mining, unmanned vehicles, surveying, defence forces, aerial photogrammetry.

In this scenario, researchers have been focusing on several aspects, such as GNSS channel modelling [6], algorithm development [7, 8], as a sensor of atmosphere [9], and receiver's performance in the challenging environments [10].

GNSS signal propagation is an important matter for the navigation system. Signal propagation can be affected by reflection, refraction, interference and diffraction phenomena. These happen when the transmitted signal faces natural or man-made obstacles along their paths. As a result, receiver receives multipath signals with different amplitudes, phases and arrival times those leads the wrong estimation about position and time [11]. Satellite antennas transmit Right Hand Circularly Polarized (RHCP) signal. Therefore, using an RHCP antenna at the receiver end gives higher received power than any other type of antenna [12].

In our measurement case, the time domain information of multipath propagated signal is not able to obtain. Received signal is the combination of line of sight (LoS) and multipath components which have been randomly summed up. The uniform geometrical theory of diffraction (UTD) has been used to model the propagation in the case of diffraction from building rooftop edge to receiver.

This thesis presents a study of diffraction and shadowing effects on GNSS received signal comparable to theoretical expectations at L1 band (1575.42 MHz).

The thesis particularly focuses on the strength of the GPS signal in LoS and NLoS case, compare the performance of Left Hand Circular Polarized (LHCP) and Right Hand Circular Polarized (RHCP) received signal and also discussion of various parameters that affect the diffraction loss.

In addition, this thesis also presents the effect of cross polarization, measurement approach, data extraction, code development including information about equipment and related measurement techniques.

This thesis work is arranged in the following chapters: Chapter 2 explains GNSS and GPS system with their operational functionalities. Chapter 3 introduces the electromagnetic wave theory and propagation mechanism including wave diffraction and polarization phenomena and also diffraction parameter V calculation from satellite azimuth and elevation angles. Chapter 5 describes the diffraction measurement scenario including measurement goals and experiment design. Chapter 6 describes the data extraction process, code development. In addition, result analysis and comparison is also presented. Chapter 7 summarizes the findings and possible improvements. Finally, conclusion of the thesis is in the Chapter 8.

2. GLOBAL NAVIGATION SATELLITE SYSTEM (GNSS)

Global Navigation Satellite System (GNSS) is a collection of satellite constellations that provide time signals from space to determine the positioning (longitude, latitude, and altitude/elevation) by its GNSS receiver. GNSS system is commonly using for accuracy (e.g. real position, speed or time), integrity (e.g. positioning data, an alarm), and seamless services in our daily life.

As of 2016 update, the United States' Global Positioning System (GPS), Russia's GLONASS, China's BeiDou Navigation Satellite System (BDS) and the European Union's Galileo are global operational GNSSs. Global coverage for each system is generally achieved by a satellite constellation of 18–30 medium Earth orbit (MEO) satellites spread between several orbital planes. The systems use orbital inclinations of >50 degrees and orbital periods of roughly twelve hours (at an altitude of about 20,000 kilometers).

The GNSS systems consist of three segments: space segment, control segment and user segment. These are illustrated in Fig. 1.

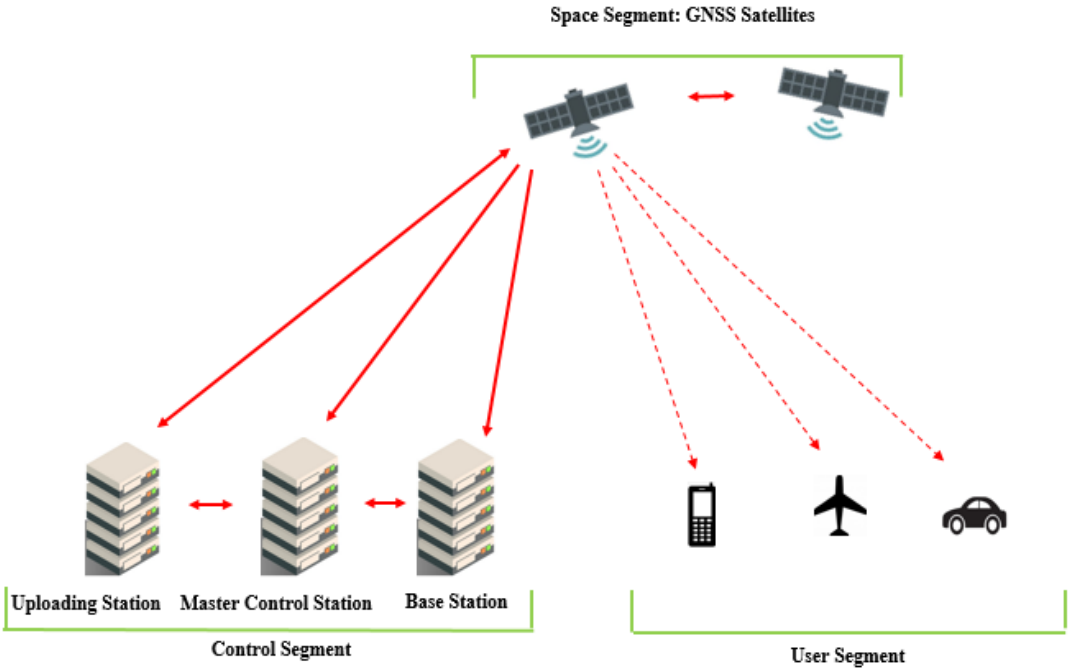

Fig. 1: GNSS system segments: space segment (upper), control segment (left) and user segment (left).

The space segment GNSS system consists of satellites, which are orbiting at the lower orbital of the earth about 20,200 km distance and provide whole coverage around the earth. Each satellite transmits identification signal including its time, orbit and status, which has a number of parameters: carrier frequency, digital codes and navigation message (as a binary phase modulation) [13].

The control segment is actually the network management equipment's on the ground such as master control stations, data uploading stations and monitor stations.

Each master control station regulates the satellite orbit parameters as well as onboard high-precision clocks. The Monitoring system gives satellite's signals and status, and send this information to the master control station. The master control station analyses the received signals then update orbit and time corrections to the satellites through data uploading stations.

The user segment refers last mile users that receive signals from the satellites and use them to determine geolocation and time information instantly. The equipment can be smartphones, smart wristwatch, receivers used for wireless connectivity survey and mapping applications etc. This thesis has been conducted from this segment where a dual polarized antenna is used to receive GPS signal.

2.1. Global Positioning System (GPS)

The Global Positioning System (GPS) is a satellite-based navigation system. The U.S. Department of defence has first developed this type of navigation system in early 1970s. Initially, GPS consists of a constellation of 24 operational satellites. These are arranged so that four satellites are placed in each of six orbitals and from any place in the world, four to ten satellites would be visible if I consider elevation angle is10°. Satellites orbits are almost circular and its maximum eccentricity is about 0.01 with an inclination of about 55° to the equator. As of May 12, 2018, a total of 31 operational satellites are in the GPS constellation [14].

2.2. GPS Operation Principle

2.2.1. GPS Signal Structure

GPS satellites broadcast microwave radio signal consisted of two frequencies (e.g. 1575.42 MHz and 1227.60 MHz) modulated by two digital code using Binary Phase Shift Keying (BPSK) and a navigation message. It's wavelength is approximately 19 cm. These two carrier frequencies allow correcting the Ionospheric delay and code modulation is different for each satellite that reduces the signal interference.

Modulation codes are known as coarse acquisition or C/A code and precision or P-code that are unique for each satellite, which assists the GPS receiver to detect which satellite is broadcasting a particular code. The bit rate of C/A and P codes are 1.023 Mbps and 10.23 Mbps respectively.

2.2.2. Distance Measurements

GNSS receiver provides three types of measurement technique: pseudo ranges (PR), Doppler frequencies (PR-rate) and carrier phases (phase).

Receiver calculates the distance between the GPS satellite's antenna and GPS receiver's antenna using either the P-code or the C/A code. The procedure can be described as follows.

Firstly, consider that both the satellite and the receiver clock are synchronized. Receiver generates an exact replica of the transmitted code from satellite that is shown in the Fig. 2. After signal travel time in space, the receiver will be picked up

that transmitted code and calculates the signal travel time by comparing the both code. Finally, obtain the range between satellite and receiver by multiplying the light velocity.

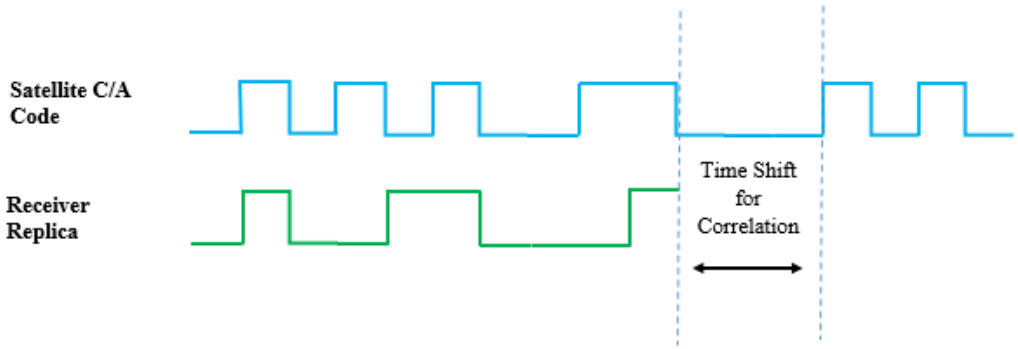

Fig. 2: Pseudo-range measurements.

2.2.3. Carrier-Phase Measurements

There is an alternative technique to measure the distance to the satellites through the carrier phases (Fig. 3). It would be the sum of the total number of full carrier cycles and fractional cycles at the receiver and satellite multiplying by carrier wavelength. This technique gives more accurate output than the pseudo-ranges method because of smaller wavelength (19 cm) than the length of pseudo range codes. But GPS receiver is not able to differentiate one cycle from another which is known as ambiguity bias [13].

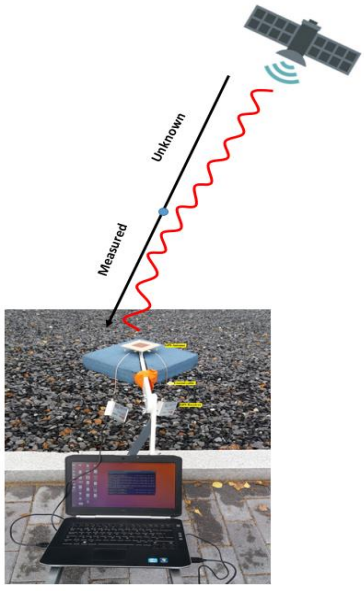

Fig. 3: Carrier-Phase measurements

2.3. GPS Inaccuracy

GPS accuracy performance depends on measurement standard as well as the strength of received signal. The satellite and receiver related atmospheric and systematic errors (Fig. 4) affect the measured accuracy of GPS receiver. Some of them are briefly discussed as follows. GPS ephemeris errors occur due to uncertainties in the solar radiation pressure model, the gravity field model, and the estimated initial state. In theoretically, it shows 2m to 5 m error. Clock error is another GPS error that causes error to the GPS measurement, which can be reduced by using Differential GNSS or Real Time Kinematic (RTK) receiver configuration. Multipath error occurs when receiver receives transmitted signal from multiple directions that can be LoS or NLoS signal from transmitter to receiver. It creates complexity for both carrier phase and pseudo-range measurements by destructing the raw signal through interference. It is more noticeable in pseudo-range measurement than carrier phase measurement. Nowadays, these type of errors have reduced dramatically using advanced receiver algorithm.

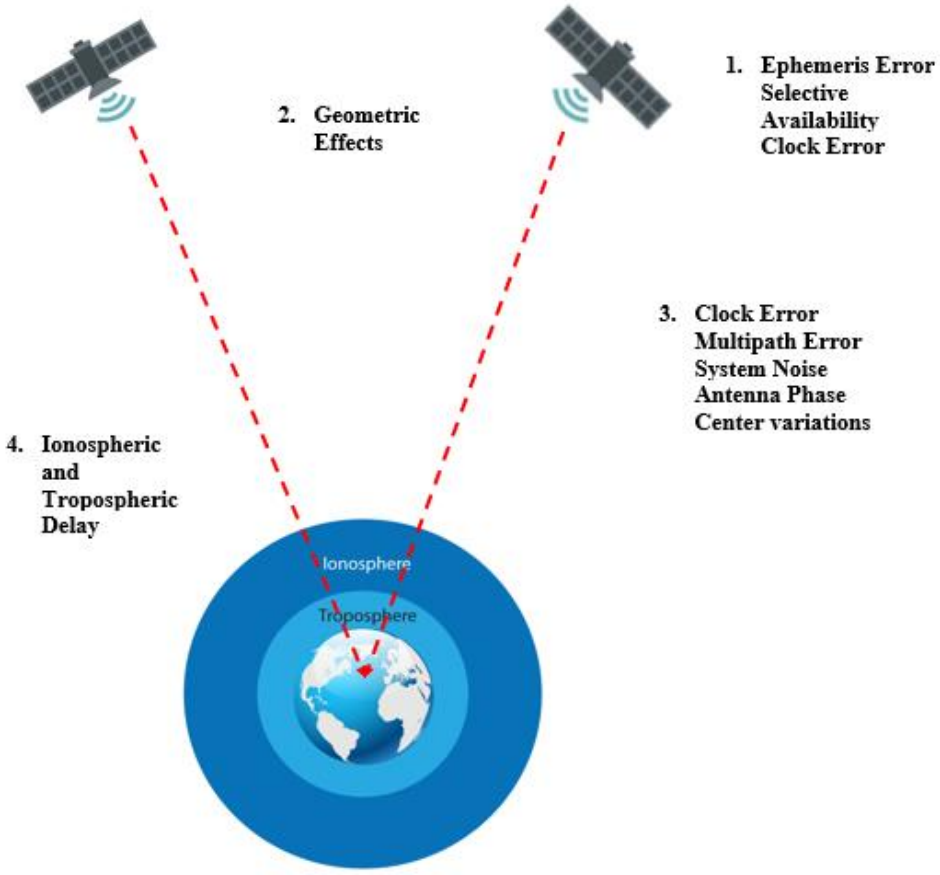

Fig. 4:GPS errors

There is another type of error occurs by the antenna-phase-center variations due to the elevation and azimuth angle of the satellite and the intensity of the observed signal.

3. ELECTROMAGNETIC WAVE (EM) AND PROPAGATION MECHANISM

3.1. Electromagnetic Wave

In 19th century, James Clerk Maxwell stated that all electromagnetic disturbances propagate in space as waves traveling at the speed of light. He showed that fluctuating magnetic fields generate associated varying electric fields, which is perpendicular to the magnetic fields. This perpendicular electric field in turn generates associated varying magnetic field in the plane of the initial magnetic field. Electromagnetic wave forms by these two varying fields that propagates at the speed of light in a direction perpendicular to both fields as shown in the Fig.5.

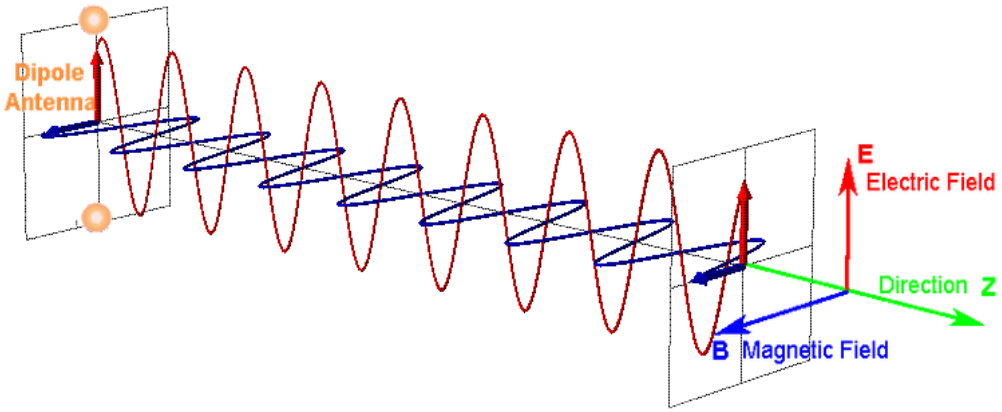

Fig. 5: Propagation of the EM wave.

3.2. Diffraction

In this chapter, I will discuss theories of diffraction including initial perception of Geometrical Theory of Diffraction (GTD) and its improvements.

In the early scientific studies of electromagnetics, there was two assumptions about light, first one assumed that light is a fluid that emerges from the eye and move along rectilinear paths toward objects. Another assumption that stated light is a radiation from the object to the eye [15].

In 1690, Huygens added his contributions to understand diffraction phenomenon which is also known as Huygens principle. He stated that a new or secondary wave front is the envelope of elementary waves emerge from the primary wave front. Although this principle was not able to explain diffraction phenomena.

In the late 17th century, Isaac Newton exposed diffraction phenomena as a new name: inflexion, which is from a Latin word inflecto that means bend. At that time, corpuscular theory of light was unable to explain the diffraction phenomena but could explain the geometrical optics phenomena such as reflection and refraction.

A.J. Fresnel merged Huygens principle with interference in 1851. He proposed that the phase of the elementary wave should be considered for secondary wave front calculation. This principle is exposed as the Huygens-Fresnel principle.

In the 19th century, Maxwell showed that there must be waves are associated with oscillating electric and magnetic fields and these waves travel at light velocity.

Italian Physicist Francesco Maria Grimaldi who had first observed diffraction phenomenon of light in 1965[16]. He demonstrated diffraction phenomenon through two experiments. The first one was light allowing passing through a small hole in direct paths blocked by a dense body. He observed that light is still bypassing that dense body and visible at outside the straight path area. In the second experiment [17], he observed that a funnel shape of light travelled through two tiny hole that produced a spot of light which is larger than the prediction according to the laws of geometrical optics (GO) or rectilinear. Grimaldi was unable to give theoretical explanation of the diffraction phenomenon although he first observed.

A simplified illustration of diffraction is shown in Fig. 6.

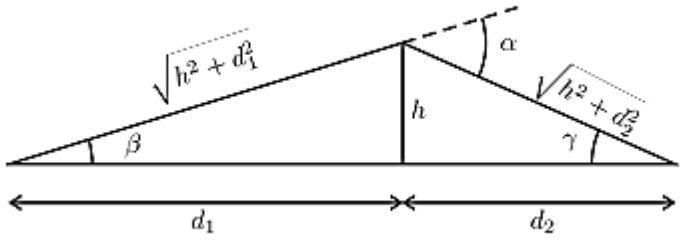

Fig. 6: Diffraction geometry

Here, finding the received signal from diffracted path is the main interest, compared to the LoS path. Because its characteristics depend strongly on the path difference Δ between diffracted and direct path. Using the geometry Δ can be expressed as follows:

$$\Delta = \frac{h^2}{2}\frac{d_1 + d_2}{d_1 d_2} \tag{1}$$

where d_1 and d_2 are the distances from the building edge to transmitter and receiver respectively.

Eq. 1 can be also written as follows:

$$\vartheta = h\sqrt{\frac{2(d_1+d_2)}{\lambda d_1 d_2}} = \alpha\sqrt{\frac{2d_1 d_2}{\lambda(d_1+d_2)}} \tag{2}$$

where ϑ is called the Fresnel diffraction parameter

Diffraction parameter, ϑ is indicated as an infinitely thin "knife edge" of diffracting object and the diffraction loss is calculated from "Fresnel integral", $F(\vartheta)$:

$$F(\vartheta) = \frac{(1+j)}{2} \int_{\vartheta}^{\infty} e^{((-j\pi t^2)/2} dt \tag{3}$$

Kirchhoff scalar theory of diffraction confirmed Fresnel's diffraction theory based on a scalar wave from a point source impinging on an opaque screen with an aperture. The layout of his experiment is shown in Fig 7. The total field at point P is given by

$$\mathbf{U(P)} = \frac{\mathbf{1}}{\mathbf{4\pi}} \int_{\mathbf{A+B+C}}^{\mathbf{0}} [\boldsymbol{u} \frac{\boldsymbol{\partial}}{\boldsymbol{\partial x}} \left(\frac{\boldsymbol{e^{-jks}}}{\boldsymbol{s}} \right) - \frac{\boldsymbol{e^{-jks}}}{\boldsymbol{s}} \frac{\boldsymbol{\partial u}}{\boldsymbol{\partial n}}] \boldsymbol{ds} \tag{4}$$

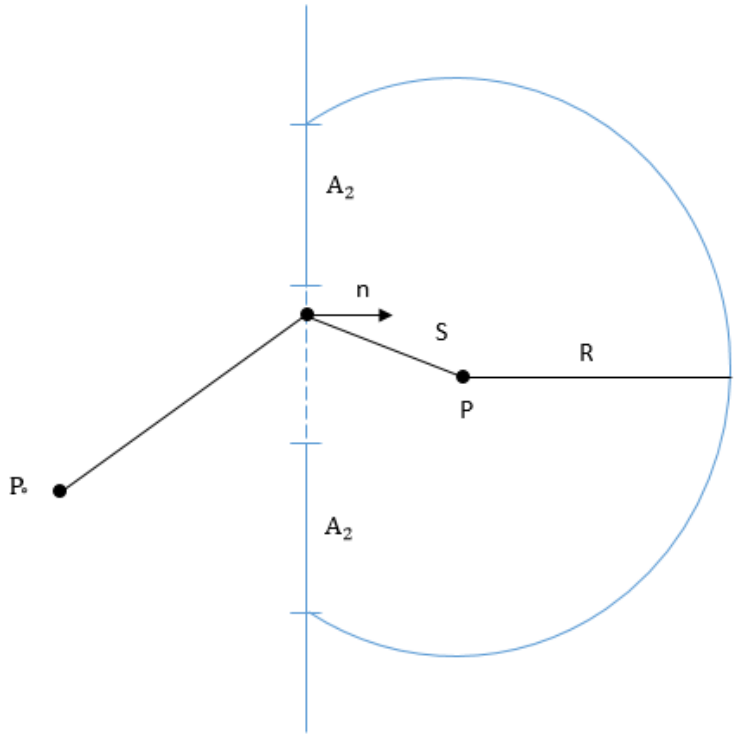

Fig. 7: Geometry of Kirchhoff's diffraction of a monochromatic wave

In 1896, Sommerfeld found that the wave in the shadow region is a cylinder-shape that comes from the edge of the half plane and the summation of a cylindrical wave and the plane wave incident can be presented as a wave in lit region. Kirchhoff explained his diffraction theory as two parts: the incident (geometrical optics) wave, u^g, and the diffracted wave, u^d, that came from the edge of the diffracting object[18], [19], [20].

Joseph Keller used the equation (4) to develop the Geometrical Theory of Diffraction [21] which has been widely used in the prediction of diffraction in wireless communication systems. He applied a modified Fermat's principle and

found that high frequency diffraction accrued is local phenomenon. Therefore, he modified this solution of scattering of electromagnetic waves from arbitrarily shaped objects to a superposition of simple canonical problems. [22].

However, there are some more improvements that are discussed as below: Kouyoumjian and Pathak develop a solution for shadow and reflection boundaries where Keller's solution failed. This is an "estimate an edge geometry by a wedge and wedge surfaces are tangent to the edge surfaces at the point of diffraction [24].

In 1984, finite conductivity and surface roughness effects added to GTD theory that is an extension of GTD wedge diffraction based on Fresnel integrals, by adding these two effects, they observe two major improvements in the prediction of diffraction loss. The first one is about the difference between the parallel and perpendicular polarization and the second is that this model is much smaller and more accurate for null depths in the interference region. Luebbers also includes the reduction in amplitude of reflection by rough wedge surface. This method is also extendable for three dimensional prediction.

3.3. Co-ordinate System: Azimuth and Elevation angle

To describe the satellite constellation's position I use spherical coordinate system(Fig. 8) that provides us the azimuth and elevation angles. Typically, most GNSS systems consider zenith axis as an elevation(el) angle of 90 degree($\theta = 90^0$) while horizone is considerd along the plane (where el = 0). GNSS co-ordinate system has been considered for the measurement and data analysis task. In the antenna co-ordinate system, zenith angle $\theta = 0^0$ for antenna.

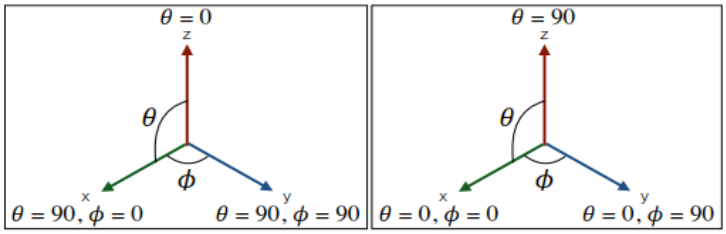

Fig. 8: Co-ordinate(left side) system for Antenna and co-ordinate system (right side)for GNSS system.

Azimuth angle is denoted by ϕ in GNSS co-ordinate system. when $\phi = 0$ which indicates to the north direction, when $\phi = 90^0$ that alignes with east direction then it goes south ($\phi = 180^0$) and west $\phi = 270^0$ direction.

3.4. Diffraction Parameter(ϑ) calculation

A knife-edge geometry is depicted in Fig.9. It is a very simple case of diffraction and there is no significant reflection can reach at the receiver end. It is considered that this sharp edge absorbs all other upcoming signals below its tip. I calculate the Fresnel Diffraction Parameter (ϑ) from the Fig: 9 based on satellite's azimuth and elevation angle. Calculation steps are described as below:

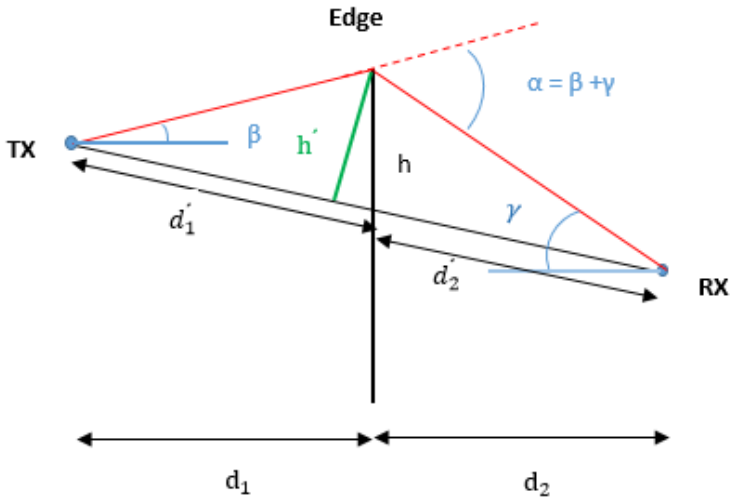

Fig. 9: Knife-edge diffraction parameters.

We know that,

Fresnel diffraction parameter can be written as(from Eq. 2),

$$\vartheta = h' \sqrt{\frac{2(d_1 + d_2)}{\lambda d_1 d_2}} \tag{5}$$

where, h' = excess height of the edge above the straight line from source to field points. ϑ is connected with $\phi = \frac{\pi}{2}\vartheta^2$. where ϕ = phase difference between the direct and reflected paths.

Firstly, I calculate receiver's azimuth angle (α) between normal and satellite that represented in the Fig: 10.

$$\theta = 270^0 - \varphi \tag{6}$$

θ varies with respect to azimuth angle of satellite (φ).

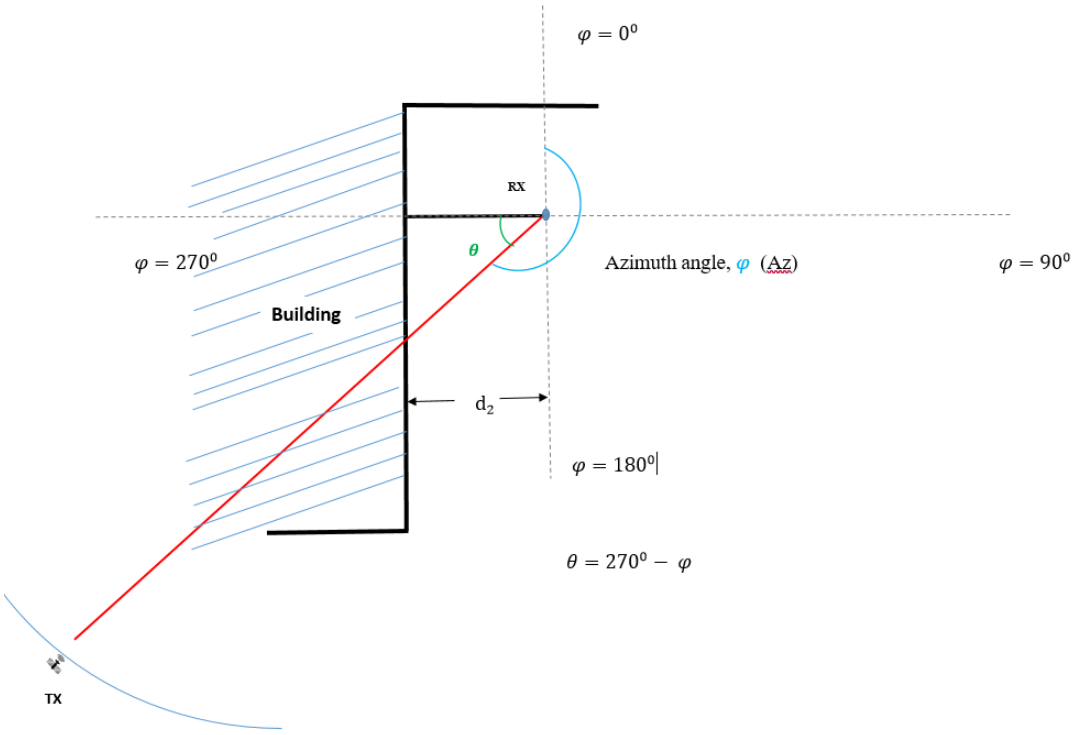

Fig. 10: Top view cut of Diffraction parameter calculation.

AB = Building height (**h**) – Receiver height from the ground(**h´´**)

= 21 m – 5.5 m = 15.5 m

Then, I calculate distance between RX and building

$$d_2 = \frac{5.5}{\cos\alpha}$$

Next, I calculate AC of Δ ACB(Fig. 11)

We know from the pythagorean theorem, $AC = \sqrt{(AB)^2+(AC)^2}$

$$AC = \sqrt{(AB)^2+(AC)^2}$$

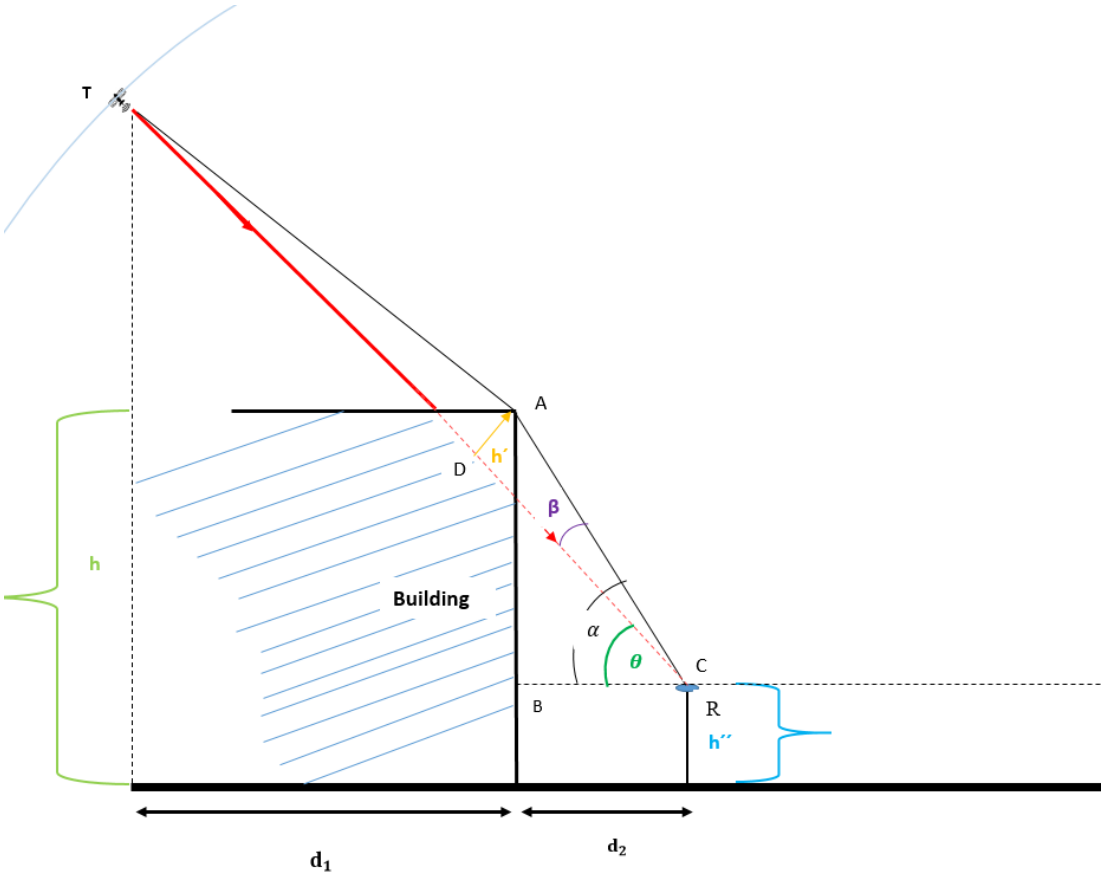

Fig. 11: Knife-edge diffraction parameter, ϑ calculation

Now, I calculate building corner angle (α) with ground, for Δ ACD I can write,

$$\alpha = \tan^{-1}\frac{h'}{d_2} \tag{7}$$

Then, $\beta = \alpha -$ Satellite elevation Angle(from measured data)

$$\text{Finally, } h' = \sin\beta \times AC$$

3.5. Right and Left Hand Circular polarization

Circularly polarized wave consists of two electromagnetic plane wave components. Both components are perpendicular to each other with equal amplitude and 90° phase difference. The electric field vector of the wave will rotate circularly in a plane which is perpendicular to the direction of propagation. If electric field vector rotates in counter clockwise with respect to the direction of propagation plane, the wave is considered as right-hand circularly polarized wave (Fig. 12) and if clockwise direction, then left-hand circularly polarized wave (Fig. 13).

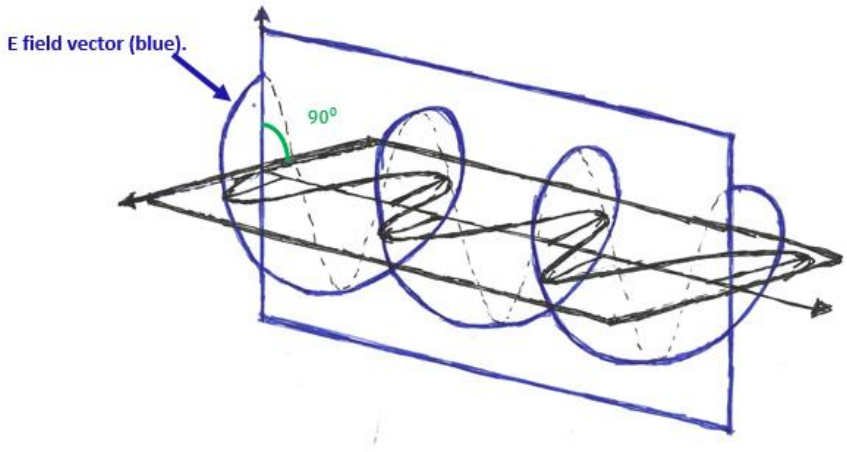

Fig. 12: Right-hand circularly (E field vector) polarized wave.

The desired signal is called the co-polar signal, whereas the unwanted signal is considered as the cross-polar signal. There are certain factors (e.g. reflections) in the propagation medium that change the polarization of the incident signals.

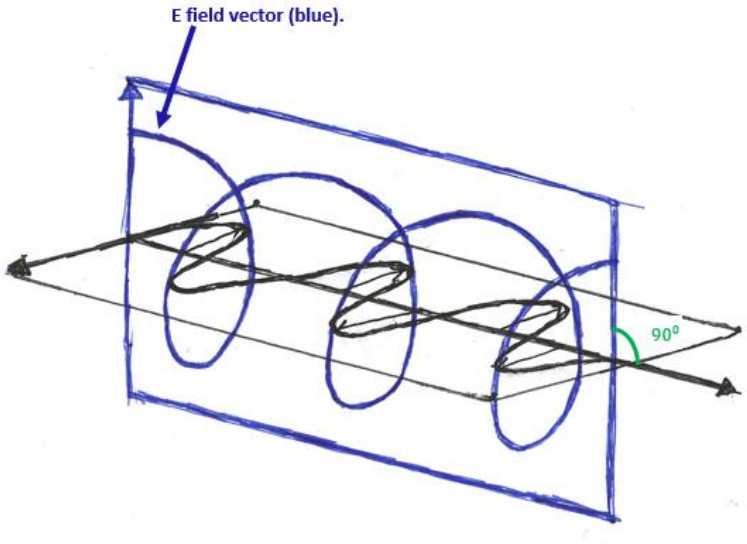

Fig.13: Left-hand circularly polarized (E field vector) wave.

3.6. Cross polarization discrimination (XPD)

The cross-polarization isolation (XPI) and the cross-polarization discrimination (XPD) tell us about the changing of signal polarization [25]. XPI describes the power

relationship of between two orthogonally polarized ports of a dual polarized antenna. XPD refers the antenna's ability (e.g. in receive mode) to sustain the incident signal's polarization purity.

XPD can be represented as follows:

$$\text{XPD} = \frac{g_{RHCP}}{g_{LHCP}} \tag{8}$$

where, g_{RHCP} and g_{LHCP} represent antennas gain in linear units.

We can write in dB,

$$\text{XPD[dB]} = 10\log\left(\frac{g_{RHCP}}{g_{LHCP}}\right) = \text{g}_{RHCP} - \text{g}_{LHCP} \tag{9}$$

Antenna radiation pattern varies in free space. XPD is the function of elevation and azimuth angle. The Elevation angle (Fig. 14) can be defined as the angle between the horizontal plane and the line of sight which is measured in the vertical plane. It is denoted by θ.

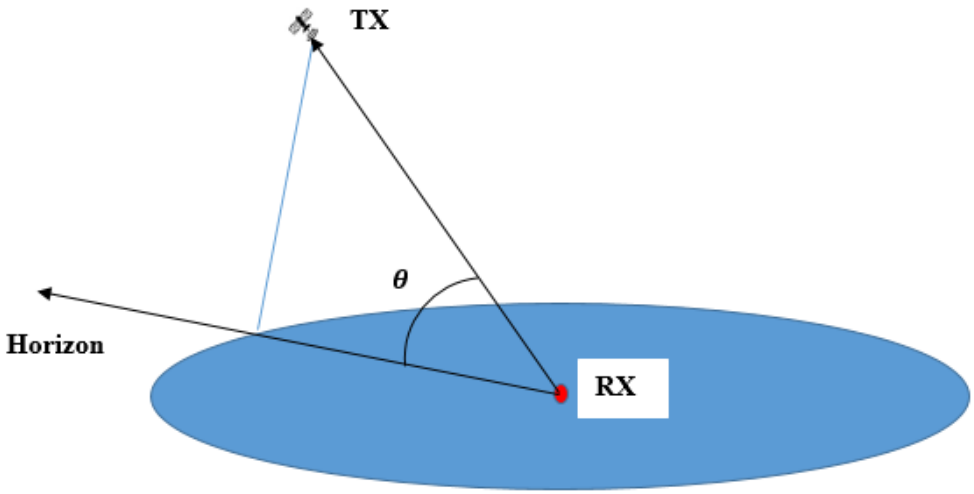

Fig. 14: Definition of elevation angle

The Azimuth angle can be defined as the 'horizontal angle' between the sources to the destination point. It is shown in the Fig. 15. In Cartesian coordinates, the azimuth angle is measured as the counterclockwise angle. . It is denoted by ϕ.

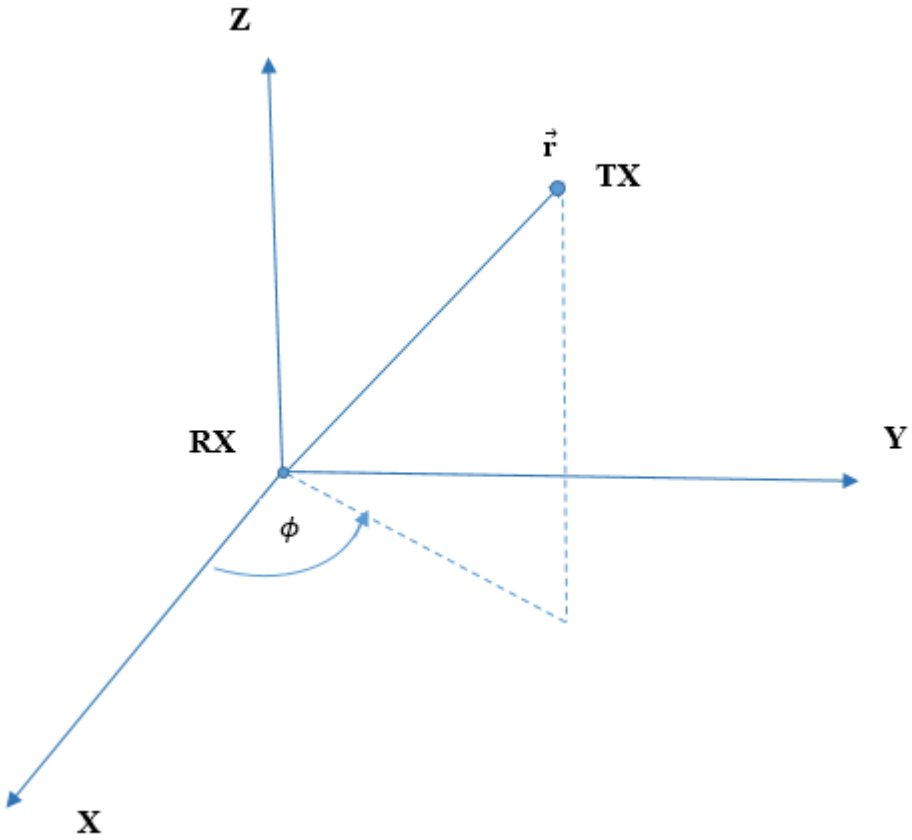

Fig. 15: Definition of Azimuth angle

Therefore, XPD can be expressed as below:

$$\begin{aligned} \mathrm{XPD}(\theta,\phi) &= 10\log\left(\frac{g_{RHCP}(\theta,\phi)}{g_{LHCP}(\theta,\phi)}\right) \\ &= \mathrm{g}_{RHCP}(\theta,\phi) - \mathrm{g}_{LHCP}(\theta,\phi) \end{aligned} \tag{10}$$

where, (θ,ϕ) means co-ordinate pair and θ represents elevation angle and ϕ represents azimuth angle.

4. ANTENNA FUNDAMENTALS

4.1. Antenna

An antenna is an important component of a wireless communications system. It uses to transmit and receive radio signals. Its operation principles are shown in the Fig. 16. Therefore, it is designed to receive guided electromagnetic waves from free space, and vice versa [26].

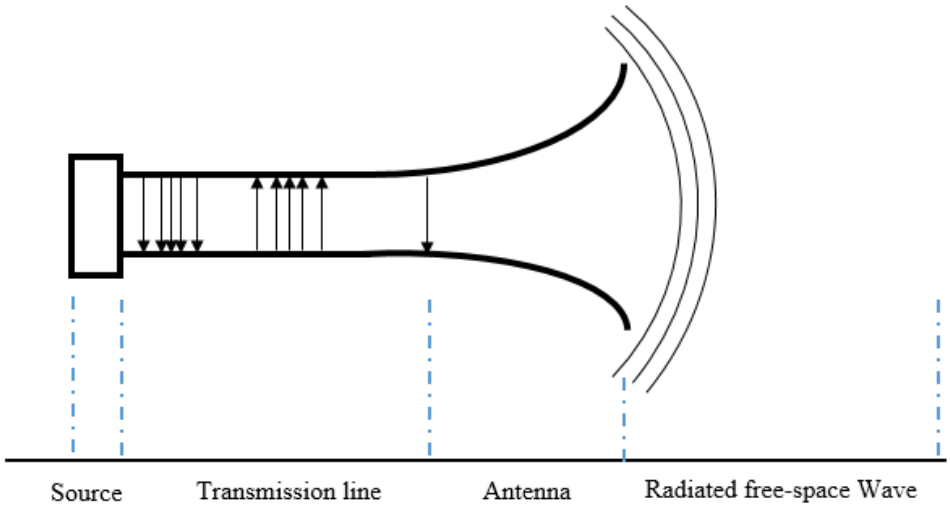

Fig. 16: Antennas operational principle in transmission

There are several types of antenna (Fig. 17) in wireless communications area that we use for different purpose, for example: wire antennas, aperture antennas, microstrip patch antennas, array antennas, reflectors antennas, lens antennas, etc.

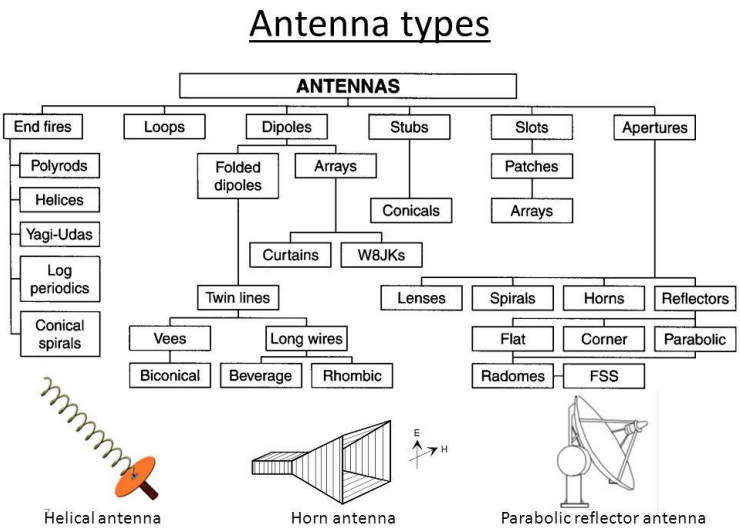

Fig. 17: Different types of Antenna.

A dual polarized patch antenna [27] has been used in the measurement that presented in the Fig.18.

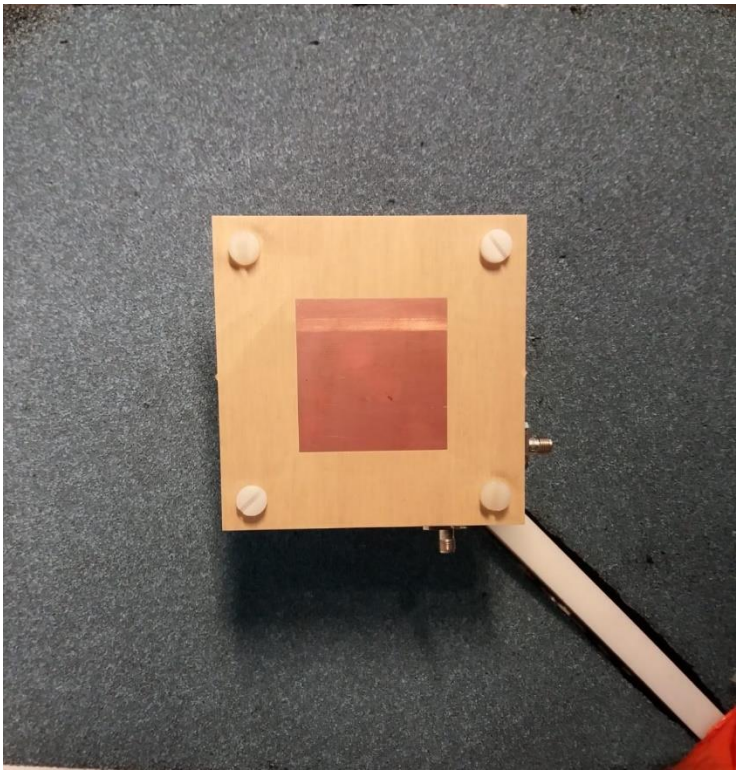

Fig. 18: Dual polarized patch antenna that used in the measurement.

The patch antenna is the most common antenna for GPS application which is less complex to mount on a flat surface, e.g. the roof top, the dashboard of the car. Patch antenna shows very high gain if they are mounted on the large ground plane. The directivity of patch antenna is maximum in zenith direction. The axial ratio of this

patch antenna is <; 1.35 for both polarizations over the 24 MHz bandwidth at the frequency of L1 band (1.575 GHz). This antenna is a low profile dual circularly polarized antenna and the cross-polarization difference is 20 dB.

The radiation pattern is also shown in the Fig.19.

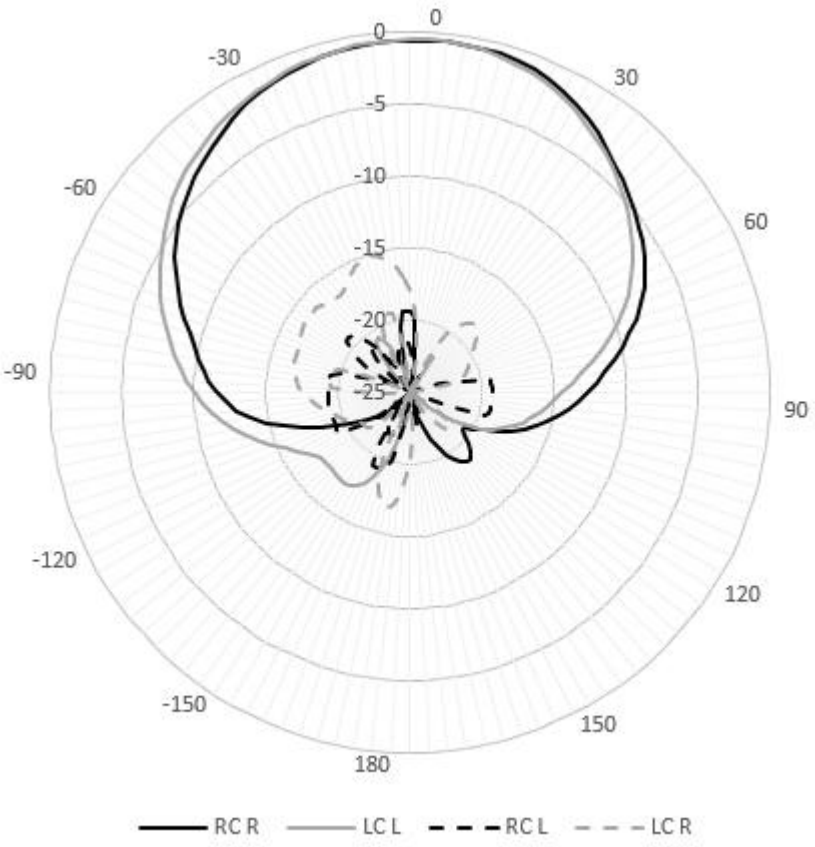

Fig. 19: Measured normalized radiation pattern of LHCP and RHCP [27].

An equivalent circuit has been shown in the Fig. 20. Antenna input impedance is defined as

$$Z_a = R_a + jX_a \tag{11}$$

where antenna resistance, $R_a = R_0 + R_r$ and X_a is antenna reactance.

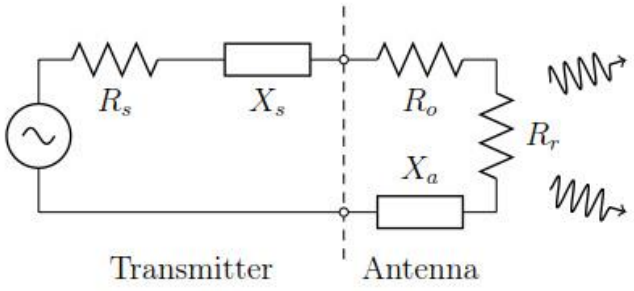

Fig. 20: An equivalent circuit of an antenna connected to a generator.

Radiation efficiency is defined as

$$\eta_{rad} = \frac{P_{rad}}{P_{in}} = \frac{R_r}{R_0 + R_r} \tag{12}$$

Radiation pattern gives information about far-field radiation properties of an antenna. It shows the strength and phase of radiation in a certain direction with respect to isotropic antenna. Normalized radiation pattern $F(\theta, \varphi)$ is expressed as a function of the azimuth angle φ and elevation angle θ:

$$F(\theta, \varphi) = \frac{E_\theta}{E_\theta(max)}, \tag{13}$$

where E_θ is the θ-component of the electrical field and its maximum value is $E_\theta(max)$.

When the antenna is conjugate matched to the source impedance $Z_S = R_S + jX_S$. It can be written as:

$$\begin{aligned} Z_S^* &= Z_a \\ R_s - jX_s &= R_a + jX_a \end{aligned} \tag{14}$$

The reflection coefficient would be zero when an antenna is perfectly matched. Reflection coefficient Γ is defined as

$$\Gamma = \frac{Z_a - Z_S^*}{Z_a + Z_s} \tag{15}$$

where Γ is the Reflection Coefficient.

5. DIFFRACTION MEASUREMENT DESCRIPTION

In this chapter, I will discuss the method and equipment that used during measurement. It also covers the goal of this measurement, geometrical layout including measurement procedure.

5.1. Measurement Operation Goal

The purpose of this measurement is to measure GPS signal while considering diffraction effect and the shadowing impact to characterize the signal attenuation. Especially, signal attenuation is characterized as a function of Fresnel diffraction parameter ϑ (depth of building edge) and the reflection in the shadow region. I have used dual polarized(e.g. RHCP and LHCP) antenna and two GNSS receivers in order to study the behaviour of the both type polarizations of received signal.

5.2. Geometrical Setup

Fig. 21 represents the geometrical setup of diffraction measurement. In the first measurement, the receiver is in a static position and the transmitter(satellite) is in moving position. Path length changes with the changing positions of the transmitter (satellite). θ_d indicates the diffraction angle.

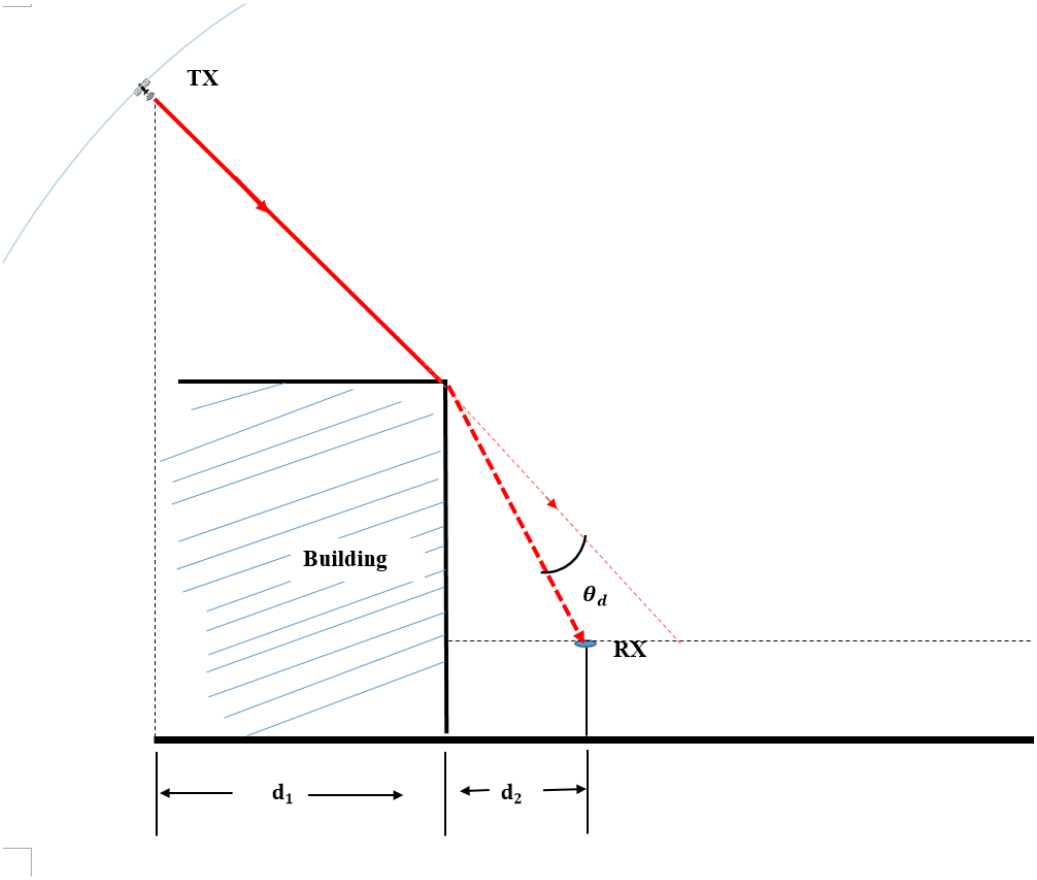

Fig. 21: Knife-edge diffraction scenario.

5.3. Measurement Procedure

First, I select a measurement location as the receiver can receive the diffracted signal in the shadow region. I prepare connection setup for the first measurement which represents in the Fig. 22.

Fig. 22: Connection setup of measurement.

Then I adjust the receiver position behind the building wall to receive the building edge diffracted signal in the shadow region. Before adjusting the receiver position, I check the availability of satellites (Fig.23) which are currently staying behind the building wall with lower elevation angle that I can extract the received signals of those satellites easily.

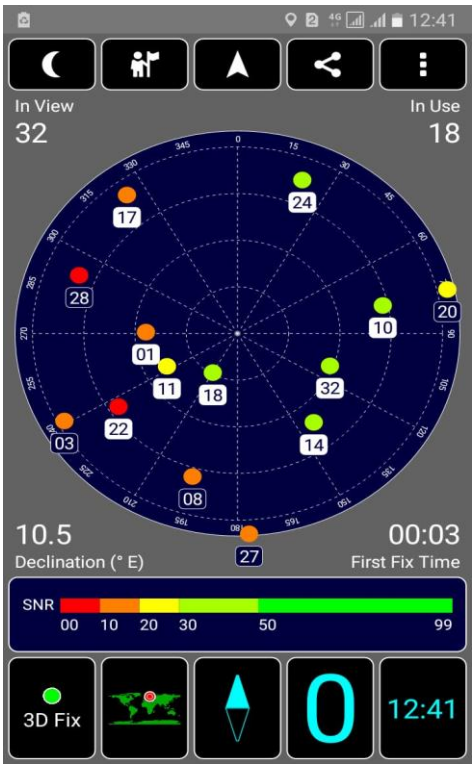

Fig. 23: Satellite constellations in polar co-ordinate system, taken from[28]

A clear line of sight measurement was done of satellite G_{12} including diffraction measurement in which knife edge diffraction has been focused. The receiver remains at the static position during the measurement. The diffracted received signal strength was very weak compared to direct signal due to diffraction Loss.

For the second scenario, I measure GPS signal while receiver is moving. I move the receiver very slowly from shadow region to LoS region that covers: shadowing effects, knife edge diffraction, and multipath propagation.

6. MEASUREMENT RESULT ANALYSIS

6.1. Data Extraction

In this measurement, I use two GNSS receivers manufactured by U-blox company and they have own evaluation sofwate named u-center. U-center software interface is shown in the Fig.24.

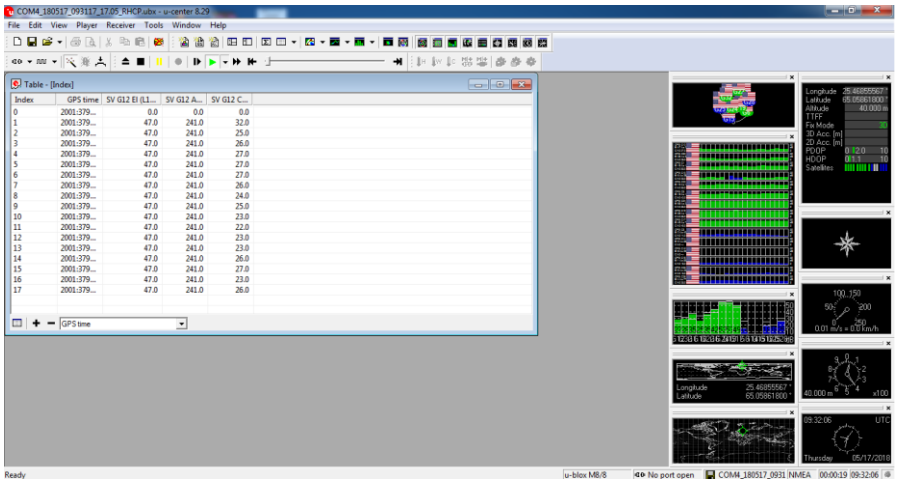

Fig. 24: Measured data extraction using U-center software.

Here, data extraction procedure is decribed as follows:

After ending of measurement, I save recoderd data file as *.ubx using u-center software. Then, Open this saved file using u-center software and select table view option from menu bar, then I select necessary features (e.g. Satellite's Azimuth and Elevation angle, C/N0, Latitude, Longitude, etc). Press the RUN button to get correspoding recorded values of selected features. Select all and save as a *.csv file.Open this *.csv file with XCEL using separations by comma and save it. It represents in the Fig.25.

	A	B	C	D	E	F	G	H	I
1	Index	UTC	Lat	Lon	SV G12 Mode (L1C/A)	SV G12 El (L1C/A)	SV G12 Az (L1C/A)	SV G12 C/N0 (L1C/A)	SV G12 Ch (L
2	0	17.5.2018 9:31	65,0586285	25,46854433	Tracking	72	137	40	
3	1	17.5.2018 9:31	65,0586275	25,468544	Tracking	47	241	32	
4	2	17.5.2018 9:31	65,05862617	25,468544	Tracking	47	241	25	
5	3	17.5.2018 9:31	65,05862483	25,46854417	Tracking	47	241	26	
6	4	17.5.2018 9:31	65,05862367	25,46854467	Tracking	47	241	27	
7	5	17.5.2018 9:31	65,05862217	25,4685455	Tracking	47	241	27	
8	6	17.5.2018 9:31	65,0586205	25,46854667	Tracking	47	241	27	
9	7	17.5.2018 9:31	65,05861983	25,46854783	Tracking	47	241	26	
10	8	17.5.2018 9:31	65,05861883	25,46854967	Tracking	47	241	24	
11	9	17.5.2018 9:31	65,05861833	25,46855083	Tracking	47	241	25	
12	10	17.5.2018 9:31	65,058618	25,46855233	Tracking	47	241	23	
13	11	17.5.2018 9:31	65,05861783	25,468553	Tracking	47	241	22	
14	12	17.5.2018 9:31	65,0586175	25,46855317	Tracking	47	241	23	
15	13	17.5.2018 9:32	65,05861767	25,46855317	Tracking	47	241	23	
16	14	17.5.2018 9:32	65,05861783	25,4685535	Tracking	47	241	26	
17	15	17.5.2018 9:32	65,05861767	25,46855433	Tracking	47	241	27	
18	16	17.5.2018 9:32	65,0586175	25,46855517	Tracking	47	241	23	
19	17	17.5.2018 9:32	65,05861767	25,4685555	Tracking	47	241	26	
20	18	17.5.2018 9:32	65,058618	25,46855583	Tracking	47	241	28	
21	19	17.5.2018 9:32	65,058618	25,46855567	Tracking	47	241	27	
22	20	17.5.2018 9:32	65,058618	25,46855583	Tracking	47	241	27	
23	21	17.5.2018 9:32	65,058618	25,4685555	Tracking	47	241	27	
24	22	17.5.2018 9:32	65,05861833	25,46855517	Tracking	47	241	27	
25	23	17.5.2018 9:32	65,0586185	25,46855483	Tracking	47	241	30	
26	24	17.5.2018 9:32	65,05861867	25,4685545	Tracking	47	241	29	
27	25	17.5.2018 9:32	65,05861883	25,468554	Tracking	47	241	20	
28	26	17.5.2018 9:32	65,05861917	25,46855367	Tracking	47	241	23	
29	27	17.5.2018 9:32	65,0586195	25,46855283	Tracking	47	241	29	
30	28	17.5.2018 9:32	65,05861967	25,46855233	Tracking	47	241	29	
31	29	17.5.2018 9:32	65,05861967	25,46855183	Tracking	47	241	28	
32	30	17.5.2018 9:32	65,05861967	25,46855217	Tracking	47	241	28	
33	31	17.5.2018 9:32	65,05861983	25,468552	Tracking	47	241	34	
34	32	17.5.2018 9:32	65,05862	25,46855233	Tracking	47	241	29	
35	33	17.5.2018 9:32	65,05862017	25,46855283	Tracking	47	241	30	
36	34	17.5.2018 9:32	65,0586205	25,468553	Tracking	47	241	34	
37	35	17.5.2018 9:32	65,058621	25,46855317	Tracking	47	241	34	
38	36	17.5.2018 9:32	65,0586215	25,46855317	Tracking	47	241	33	
39	37	17.5.2018 9:32	65,05862183	25,46855283	Tracking	47	241	33	
40	38	17.5.2018 9:32	65,058622	25,46855317	Tracking	47	241	32	
41	39	17.5.2018 9:32	65,05862217	25,4685535	Tracking	47	241	31	
42	40	17.5.2018 9:32	65,0586225	25,46855317	Tracking	47	241	31	
43	41	17.5.2018 9:32	65,05862267	25,4685525	Tracking	47	241	30	

Fig. 25: Data conversion in excel for MATLAB use.

6.2. Code development

A MATLAB code[Appendix 1] has been developed to calculate the Fresnel Diffraction parameter(Eq. 2, and 7) in the case of the knife-edge diffraction model[29,30] to observe the signal attenuation. Satellite is moving continuously that changes the elevation and azimuth angle. So that, propagation path length, diffraction angle, relative distance between RX and building edge, and distance from the satellite to building edge changes. The measurement was recorded for two hours and received more than six thousand value for each item which is totally impossible to manually calculate the diffraction related parameters. All calculations and plots have been done using this code. Calculation steps also have presented in the next subchapter.

6.3. Measurement Results

In the first measurement, I have recorded GPS signal (satellite G_{12}) for two hours where satellite's elevation angle started from 47° and finally reached at 76° maximum and the azimuth angle range was 241° to 137°. Fig. 26 illustrates the knife-edge attenuation of received GPS signal with respect to Fresnel diffraction

parameter (ϑ). In this Fig. 26, Fresnel diffraction parameter (ϑ) indicates the receiver's position within the shadowed region.

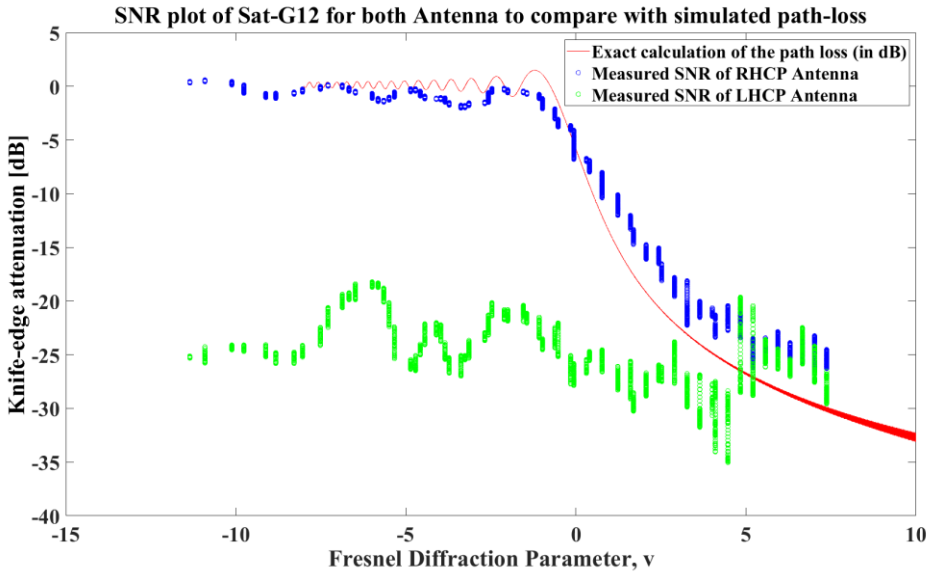

Fig. 26: Simulation and measurement results while receiver is at the static position: RHCP (blue) and LHCP (green)

The zero value of ϑ means that the transmitter, receiver and spike of the building all are in the same line and the electric field strength is theoretically decreased by half or the power is decreased to one fourth of the value without the obstruction i.e. a loss of 6 dB. A negative value of ϑ indicates the line of sight propagation between transmitter and receiver where obstacle is below the line of sight. Typically, there is no loss in this region. As the value of the v increases on the positive side that leads NLoS propagation. For this reason, attenuation reaches sharply in of range of 25dB to 30 dB. I normalize our measured raw data to find out the correlations among them and use moving average filter (window size = 100) to remove noise from the raw data.

It can be seen from the Fig.26, in the LoS propagation, the received signal pattern (blue color) of the RHCP antenna shows an 'interference pattern (constructive and destructive)' because of multipath effect (Fig. 27), and the signal is strong enough for successful acquisition and tracking processes.

Fig. 27: Diffraction measurement location while RX is in static position (RX can receive multipath signal), taken from google map.

The noticeable thing is that the 'interference pattern' of the measured signal in LoS zone is much slower than the simulated pattern. Possible cause of this pattern could be the less or extreme multipath signal receives at that position. At the near end of LoS zone (ϑ = -2.5 to -0.50), signal strength decreases due to diffraction losses. In contrast, LHCP antenna receives weak signal because of cross polarization which XPD is approximately 20 to 25dB.

In NLoS propagation, received signal strength of RHCP antenna decreases with increasing the depth of building edge because of diffraction by the building edge. Therefore, RHCP antenna receives delayed and weak signal in the deep shadow region due to diffraction losses that causes precision errors [31].

From the Fig.26 it can be observed that signal strength of the LHCP antenna slightly increases in the deep shadow region which is equal to the received Signal-to-Noise Ratio (SNR) of RHCP antenna. Hence, Both RHCP and LHCP antennas receive linearly polarized signal in deep shadow region (ϑ = 5 to 7.50).

There are two possible reasons behind this characteristic of the received signal. Firstly, the LHCP antenna receives a reflected signal from other obstructions (e.g. trees), after reflection RHCP signal becomes a LHCP signal which has shown in the below Fig.28.

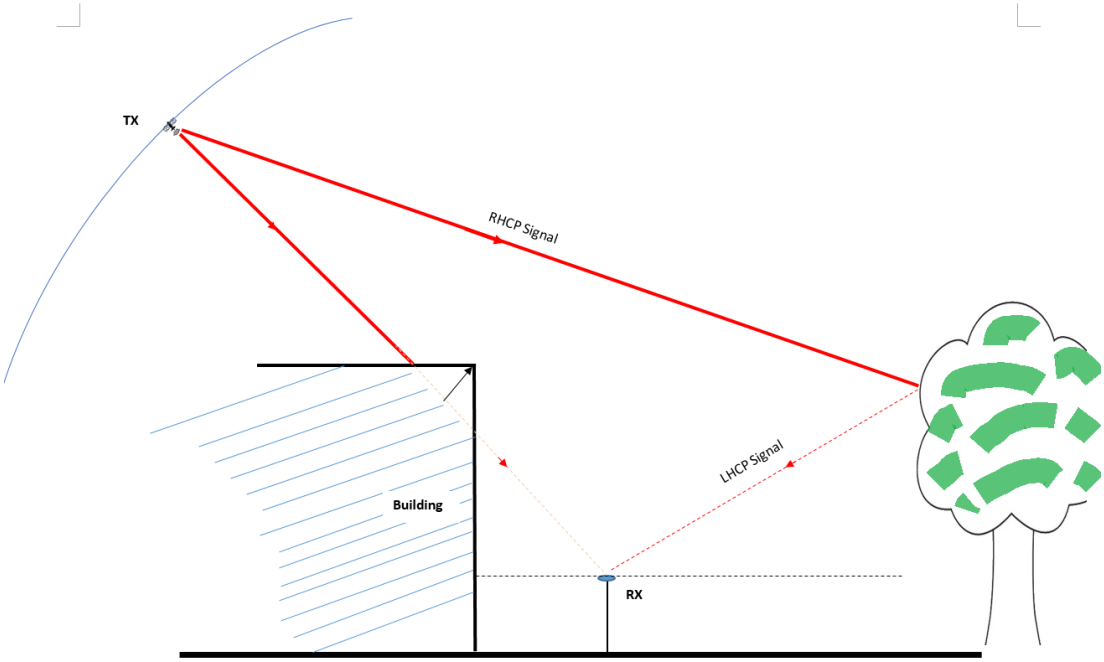

Fig. 28: LHCP antenna is receiving reflected signal from trees.

Secondly, as I know from the boundary conditions: only the perpendicular components of incident EM wave do not collapse and continue along the surface of an ideal conductor although the parallel component vanishes [31]. Therefore I get almost the same strength signal for both antennas in the shadow region. Circular polarization consists of two orthogonal linear polarized waves (90 degrees out of phase). After diffraction, the circularly polarized both antenna receive the linearly polarized wave (Fig. 29) and it shows nearly the same signal strength for both antenna (RHCP and LHCP) which is visible in the Fig. 26.

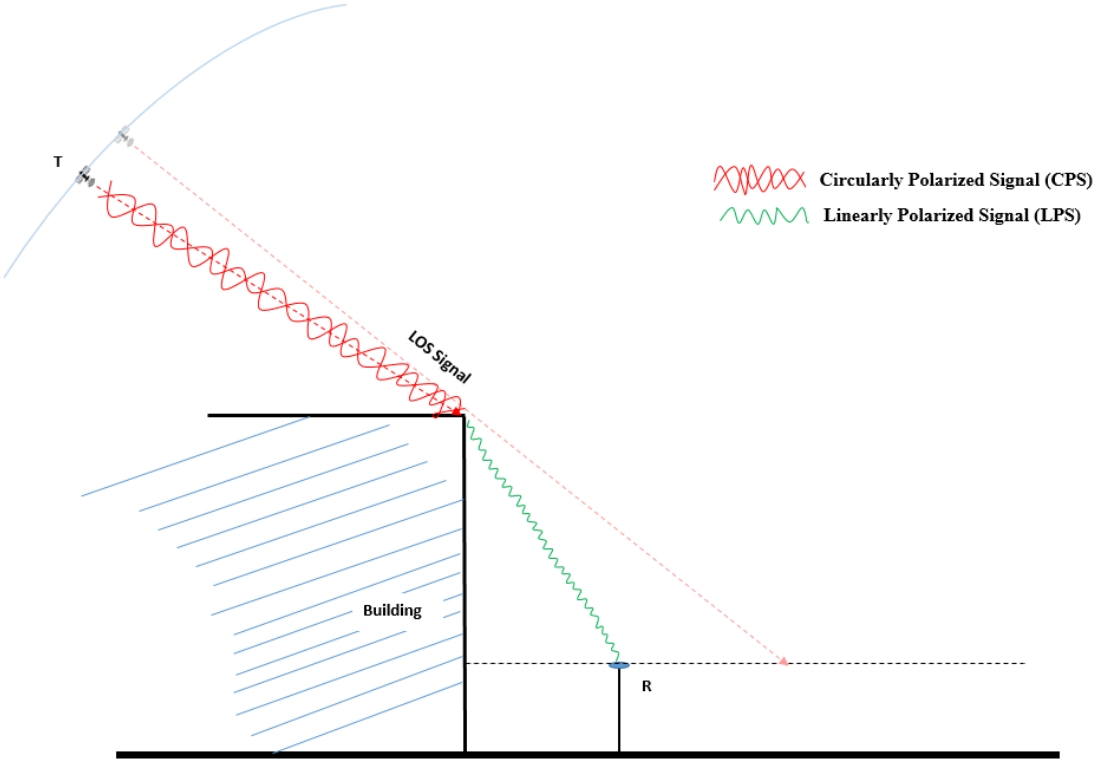

Fig. 29: Antenna is receiving diffracted signal as a linearly polarized signal.

However, polarization does not affect extremely on diffraction losses [32]. It can be observed from the Fig. 26, both antennas receive almost same SNR of diffracted signal in shadow region (ϑ = 5 to 8) which is linearly polarized signal (polarization changed). It may suffer 3dB loss due to polarization mismatch.

In the Table.1, signal to noise ratio (SNR) has been calculated using antenna gain and received SNR. Antenna receives different SNR with respect to satellite's elevation angle. Antenna gain can be found from the radiation pattern that is shown in Fig.18.

Table 1: Real SNR calculation

Elevation Angle(degree)	Measured SNR(dB)	Antenna Gain(dB)	Real SNR(dB)
48	29.1125	-5.36886	34.4813
51	30.2083	-4.70225	34.91055
54	30.95	-4.04236	34.99236
57	33.7813	-3.39776	37.17906
60	36.2583	-2.77477	39.03307
63	42.4625	-2.17614	44.63864
66	48.225	-1.60239	49.82739
69	54.10	-1.05182	55.15182
72	53.525	-0.52152	54.04652
75	54.5375	-0.00909	54.54659
78	54.7167	0.48653	54.23017

I took second measurement while receiver was in motion and the measurement location is shown in the Fig. 30. In this second measurement, GPS signal (satellite G_{27}) had been recorded for ten minutes where satellite's elevation angle varies from 58° to 62° and the azimuth angle range along from 271° to 264°.

Fig. 30: Diffraction measurement location while RX is moving from NLoS to LoS propagation, taken from google map.

Fig. 31 is the measured signal for both antenna while receiver is moving slowly from NLoS to LoS region. In this case, it can also be seen that the knife-edge attenuation due to the building edge diffraction. Moving average filter (window size = 10) has been used to remove noise from the raw data.

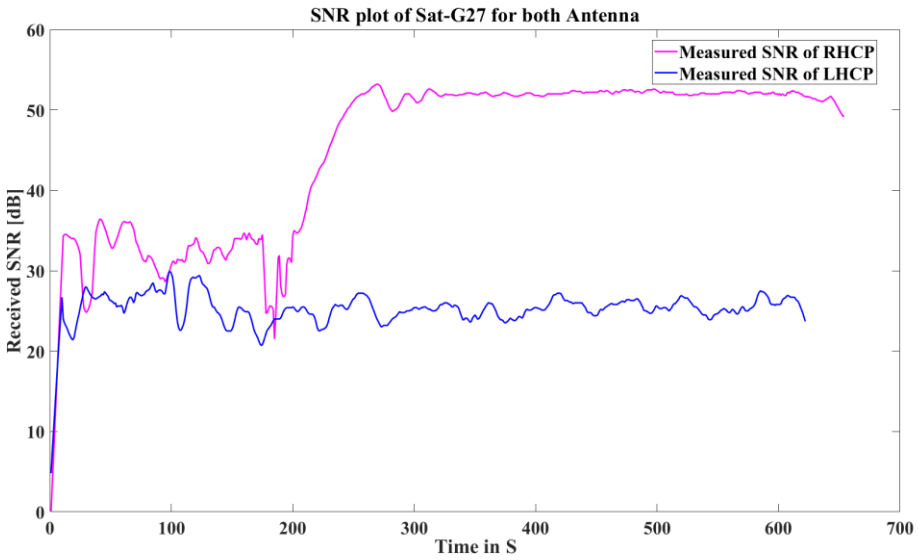

Fig. 31: Recorded GPS signal while receiver is in dynamic position: RHCP (purple) and LHCP (blue).

In shadow region, there are huge fluctuations in received signal of both antennas which is visible in the Fig. 31. It fluctuates from -22 to -38 dB. Note that, both antennas receive diffracted and reflected (e.g. from my body while pulling antennae) signal in NLoS propagation. It can be clearly observed that interference fringes are irregular and have rapid fluctuations with respect to time.

At the beginning of LoS propagation (t = 275 s to 300 s), RHCP antenna receives the direct signal from a satellite which gives higher peak than other constructive fringes that can be seen from the Fig.30 and signal attenuation due to knife-edge diffraction is similar to double edge diffraction pattern[32]. On the other hand, LHCP antenna receives a certain level signal due to the XPD which is acceptable. For rest of the time (LoS), received signal level of the RHCP antenna is about 52 dB. LHCP antenna receives a certain level signal (25 to 30 dB) during whole measurement time.

7. DISCUSSION

These measurements have been conducted to investigate the impact of diffraction and shadowing on the received GNSS signal. Both the measurement procedure and systems worked effectively to study predetermined objectives. Finally, these measurements were succesfull and obtained good result which agreed with the theory. However, several issues can be tuned up to get better location accuracy for GNSS applications. A well-organized arrangement such as ideal location selection might be effective to get accuracy in measurement. A few improvements for future work are explored further.

7.1. Imrovements of Measurement setup and Antenna Selection

This measurement setup conceded very good agreement between theoretical and practical results even though other modifications and ideal measurement scenarios can improve the accuracy of results in further measurement. The measurement has been executed in the public place and its surroundings were populated(e.g. people, bicycle) during measurement time. Therefore, the effect of environment was very difficult to avoid during measurement. An ideal location can be selected for further measurement. However, a high gain antenna can be used to receive the signal in the shadow region that covers other GNSS systems(e.g. GLONASS, Galileo). Positioning errors occur due to multipath reflections from nearby or far objects. Therefore, choosing a suitable antenna can be a better solution to reject the multipath signal. The antenna should be mounted as near to the horizontal surface as possible(at low elevation angle) and away from reflecting objects (e.g. antenna holding stuff, metal) to suppress the multipath signal from the ground and other objects. The axial ratio(AR) of the antenna should close to 1(or 0 dB) that means a good circular polarization. The XPD of the antennas was more than 20dB which is acceptable for this measurement.

7.2. Possible Implentation

In future, these measurements can be performed using a choke ring antenna that offers high multipath rejection due to unique concentric ring design and block out multipath signal reflection. Using drone can be added in the further measurement that would be effective for unmanned aerial vehicle (UAV) communication.

8. CONCLUSION

This thesis discusses the effect of diffraction and shadowing on the GNSS received signal. The experiment demonstrates a very good agreement between the measured and theoretically simulated knife-edge attenuation due to the diffraction. It also reviews the electromagnetic wave theory, related antenna theory. Measurement has performed in two different case (i) receiver was in static position and (ii) receiver was in motion. A description of diffraction parameter calculation and discussion comes in Chapter 6 including MATLAB code.

The effect of knife-edge diffraction is clearly observable in the characterization of signal attenuation. Received signal strength has decreased by half (6 dB) while the transmitter, receiver, and edge of the building are all on the same line (diffraction parameter ϑ is zero).

Both RHCP and LHCP antennas receive same SNR in the shadow region. It seems that received signal is linearly polarized.

9. REFERENCES

[1] Fontana R, Cheung W, Novak P, Stansell T. The New L2 civil signal. Proceedings of U.S. Institute of Navigation, Salt Lake City, UT, 11–14 September 2001; 617–631.

[2] D.N. Aloi ; F. Van Graas, Year: 2004 , Volume: 40 , Issue: 2 Page s: 536-552. Ground-multi path mitigation via polarization steering of GPS signal.

[3] P. Axelrad ; C.J. Comp ; P.F. Macdoran, Year: 1996 , Volume: 32 , Issue: 2 Page s: 650 - 660. SNR-based multipath error correction for GPS differential phase.

[4] A.El-Rabbani. 2002; Introduction to GPS, P-2.

[5] A.El-Rabbani. 2002; Introduction to GPS, P-7

[6] A. Bourdeau, M. Sahmoudi, J.-Y. Tourneret- ION GNSS, 2012.Tight Integration of GNSS and a 3D City Model for Robust Positioning in Urban Canyons.

[7] R. Kumar, MG Petovello. ION GNSS, 2014, Session D6, Tampa, FL, 8 - 12 September 2014. A novel GNSS positioning technique for improved accuracy in urban canyon scenarios using 3D city model.

[8] Nainesh Agarwala, Julien Bascha, Paul Beckmanna, Piyush Bhartia, Scott Bloebauma; (2002). Algorithms for GPS Operation Indoors and Downtown.

[9] Maiying Zhong; Jia Guo; Zhaohua Yang; (2016). On Real Time Performance Evaluation of the Inertial Sensors for INS/GPS Integrated Systems.

[10] C. Cristodaro; F. Dovis; Gianluca Falco; 2017. GNSS receiver performance in urban environment: Challenges and test approaches for automotive applications.

[11] M. Andreotti; M. Aquino; M. Woolfson; J. Walker; T. Moore 2006 IEEE/ION Position, Location, And Navigation Symposium. Signal Propagation Analysis and Signature Extraction for GNSS Indoor Positioning.

[12] Polarization based measurement system for analysis of GNSS multipath signals Markus Berg ; Rameez UR Rahman Lighari ; Jani Kallankari ; Ville Majava ; Aarno Pärssinen ; Erkki T. Salonen 2016 10th European Conference on Antennas and Propagation (EuCAP).

[13] A. El-Rabbani. 2002; Introduction to GPS, pp.09.

[14] GPS official website: https://www.gps.gov/systems/gps/space/(Accessed:

November 15, 2018).)

[15] W.F. Croswell, O.M. Bucci, and G. PeLoSi, “From Wave Theory to Ray Optics,” IEEE Antennas and Propagat. Mag., Vol. 36, No.4, pp. 35-42, Aug. 1994.

[16] F.M. Grimaldi, De Lumine, 1665.

[17] J. Griffiths, Radio Wave Propagation and Antennas, Englewood Cliffs, NJ: Prentice-Hall, 1987.

[18] K. Miyamoto and E. Wolf, “Generalization of the Maggi-Rubinowicz Theory of Boundary Diffraction Wave, Part I,” J. Optical Soc. of America, vol. 52, no. 6, pp. 615-625, 1962.

[19] K. Miyamoto and E. Wolf, “Generalization of the Maggi-Rubinowicz Theory of Boundary Diffraction Wave, Part II,” J. Optical Soc. of America, vol. 52, no. 6, pp. 626-637, 1962.

[20] A. Rubinowicz, “Zur Kirchhoffschen Beugungstheorie,” Annalen der Physik, vol. 73, no. 4, pp. 339-364, 1924.

[21] W.F. Croswell, O.M. Bucci, and G. PeLoSi, “From Wave Theory to Ray Optics,” IEEE Antennas and Propagat. Mag., Vol. 36, No.4, pp. 35-42, Aug. 1994.

[22] W.F. Croswell, O.M. Bucci, and G. PeLoSi, “From Wave Theory to Ray Optics,” IEEE Antennas and Propagat. Mag., Vol. 36, No.4, pp. 35-42, Aug. 1994.

[23] J.B. Keller, “Geometrical Theory of Diffraction,” J. Opt. Soc. of America, vol. 52, no. 2, pp. 116-130, Feb. 1962.

[24] R.G Kouyoumjian, and P.H. Pathak, “A Uniform Geometrical Theory of Diffraction for an Edge in a Perfectly Conducting Surface,” Proc. IEEE, vol. 62, no. 11, pp. 1448-1461, Nov. 1974.

[25] G. Maral and M. Bousquet, Satellite Communications Systems: Systems, Techniques and Technology, 4th ed. John Wiley and Sons, 2002.

[26] J. Holopainen, “Compact UHF-band antennas for mobile terminals: Focus on modelling, implementation, and user interaction”, Doctoral dissertation, Aalto University, 2011, 86 pages.

[27] Markus Berg; Rameez Ur Rahman Lighari ; Tommi Tuovinen ; Erkki T. Salonen (2016). Circularly polarized GPS antenna for simultaneous LHCP and RHCP reception with high isolation.

[28] GPS Test software(android version).

[29] Lee W C Y ,Mobile Communications Engineering 1985. Calculation of the path loss based on the value of Fresnel Diffraction Parameter

[30] http://www.raymaps.com/index.php/knife-edge-diffraction-model/

[31] R. Luebbers, Year: 1984 , Volume: 32 , Issue: 1 Page s: 70 – 76. Finite conductivity uniform GTD versus knife edge diffraction in prediction of propagation path loss.

[32] Albert G. Gluckman. Nov 1989. On Multiple Edge Diffraction and Multiple Reflections of Microwaves over Terrain.

Appendix 1

```
% This code calculates the Fresnel Diffraction parameter, V.

d1 = 20000000;% Distance of satellite
h = 15.5; % building height
snr = xlsread('sat_12.xlsx', 'I:I'); % SNR of G_12 satellite

%A moving-average filter.
windowSize = 100;
b = (1/windowSize)*ones(1,windowSize);
a = 1;
B = filter(b,a,snr);
snr2 = B - 55;
el = xlsread('sat_12.xlsx', 'G:G'); % Elevation angle of G_12
satllite
az = xlsread('sat_12.xlsx', 'H:H'); % Elevation angle from
received data, column
alfa = 270 - az; % Rx's azimuth angle between normal and satellite
k = cos(degtorad(alfa));
d_2 = 5.5./k; % distance between Rx and building

hypotenus = sqrt(h^2 + d_2.^2); % Using Pythagorean theorem

angle = radtodeg(atan(h./d_2)); % building corner angle with
ground

beta = angle - el;
h_prime = sin(degtorad(beta)).*hypotenus;

lambda = 0.19; %wavelength in meters
v = h_prime.*abs(sqrt(2*(d1+d_2)./(lambda*d1*d_2))); % Fresnel
Diffraction parameter

v2 = -8:0.01:10;

for n=1:length(v2)

    v_vec = v2(n):0.01:v2(n)+100;

    S(n)=((1+1i)/2)*sum(exp((-1i*pi*(v_vec).^2)/2));

end

S = abs(S)/(abs(S(1)));
plot(v2, 20*log10(S),'r');
hold on
scatter(v(100:4500,1),snr2(100:4500,1), 'b');
legend('Exact calculation of the path loss (in dB)based on Fresnel
Diffraction Parameter (v)');
xlabel('Fresnel Diffraction Parameter, v')
ylabel('Knife-edge attenuation [-dB]')
```